nature neuroscience

Sensory cortex limits cortical maps and drives top-down plasticity in thalamocortical circuits

Andreas Zembrzycki[1], Shen-Ju Chou[1,3], Ruth Ashery-Padan[2,3], Anastassia Stoykova[2] & Dennis D M O'Leary[1]

The primary somatosensory cortex (S1) contains a complete body map that mirrors the subcortical maps developed by peripheral sensory input projecting to the sensory hindbrain, the thalamus and then S1. Peripheral changes during development alter these maps through 'bottom-up' plasticity. Unknown is how S1 size influences map organization and whether an altered S1 map feeds back to affect subcortical maps. We show that the size of S1 in mice is significantly reduced by cortex-specific deletion of *Pax6*, resulting in a reduced body map and loss of body representations by an exclusion of later-differentiating sensory thalamocortical input. An initially normal sensory thalamus was repatterned to match the aberrant S1 map by apoptotic deletion of thalamic neurons representing body parts with axons excluded from S1. Deleted representations were rescued by altering competition between thalamocortical axons using sensory deprivation or increasing the size of S1. Thus, S1 size determined the resolution and completeness of body maps and engaged 'top-down' plasticity that repatterned the sensory thalamus to match S1.

In mammals, sensory stimuli originating from peripheral sensory organs or receptors are relayed to the neocortex, where they are processed in modality-specific primary and higher-order sensory areas and brought to perception[1,2]. The sensory periphery is represented in the primary sensory areas in organized maps. For example, tactile receptors distributed over the body are represented in somatotopic maps in S1 (refs. 3,4). The size of the representation of a body part in the S1 cortical map relates directly to the relative number and density of peripheral sensory receptors that innervate that body part[3,5]. This relationship results in the body representation in S1 being organized into a distorted somatotopic map, with body parts disproportionally represented on the basis of innervation density rather than size of the body part. Similar body maps are also evident in subcortical sensory nuclei that connect the sensory periphery to S1, first in hindbrain sensory nuclei and ultimately through the projection of thalamocortical axons (TCAs) from the ventroposterior thalamic sensory nucleus (VPN) developing in a peripheral-to-central, or bottom-up, progression[6–10] (**Supplementary Fig. 1**).

The sensory map in a primary cortical area is malleable in both the adult and developing brain and shows plasticity in its organization in response to manipulations of the sensory periphery[3,4,11–13]. Plasticity in sensory maps has been studied most intensively in the somatosensory system of mice because the body map can be revealed using anatomical methods that relate directly to its functional representations throughout the brain, and the body map can be reproducibly manipulated peripherally with sensory deprivation and centrally with genetic approaches. Development of a normal body map in S1 requires an intact sensory periphery and connectivity from the periphery through to cortex during a critical period of development. Manipulations of the sensory periphery during this critical period that result in sensory deprivation—for example, removal of sensory innervation to a body part—produce a defect or absence of representation of the deprived body part in subcortical and S1 cortical body maps. Similarly to map development, this plasticity proceeds in a peripheral-to-central or bottom-up progression[3,4], beginning with a defective body map in sensory hindbrain nuclei, which moves to the VPN thalamus and then the S1 cortex[14].

In contrast to the vast literature on bottom-up plasticity[3,4,8–10,15], little is known about how the size of a primary sensory area influences the cortical representation of the sensory periphery and whether an altered cortical representation might engage a top-down plasticity. These issues are of particular importance because the sizes of primary areas in humans reportedly vary as much as 200% across the normal population[16–18], and more sizeable differences are present in individuals with developmental trauma or congenital defects of the cortex, which can result in behavioral deficits and neural dysfunction[19,20]. Further, tactile and motor behaviors are degraded in adult mice when sensorimotor areas are either reduced or increased in size by embryonic genetic manipulations[21] or disconnected from the thalamus[22]. Here we use the mouse somatosensory system as a model to address the influence of cortical area size on sensory representations and the potential for top-down plasticity to modify subcortical sensory nuclei in response to changes in S1.

RESULTS

Cortex-specific deletion of *Pax6* reduces S1 size

Transcription factors expressed by cortical progenitors regulate area size and position[23]. A role for the transcription factor Pax6 in preferentially specifying sensorimotor areas has been suggested by analyses of small eye–mutant mice that lack functional Pax6 protein[24],

[1]Molecular Neurobiology Laboratory, The Salk Institute For Biological Studies, La Jolla, California, USA. [2]Department of Molecular Cell Biology, Max Planck Institute for Biophysical Chemistry, Goettingen, Germany. [3]Present addresses: Institute of Cellular and Organismic Biology, Academia Sinica, Taipei, Taiwan (S.-J.C.) and Department of Human Molecular Genetics and Biochemistry, Sackler Faculty of Medicine, Tel Aviv University, Tel Aviv, Israel (R.A.-P). Correspondence should be addressed to D.D.M.O. (doleary@salk.edu).

Received 28 December 2012; accepted 6 June 2013; published online 7 July 2013; doi:10.1038/nn.3454

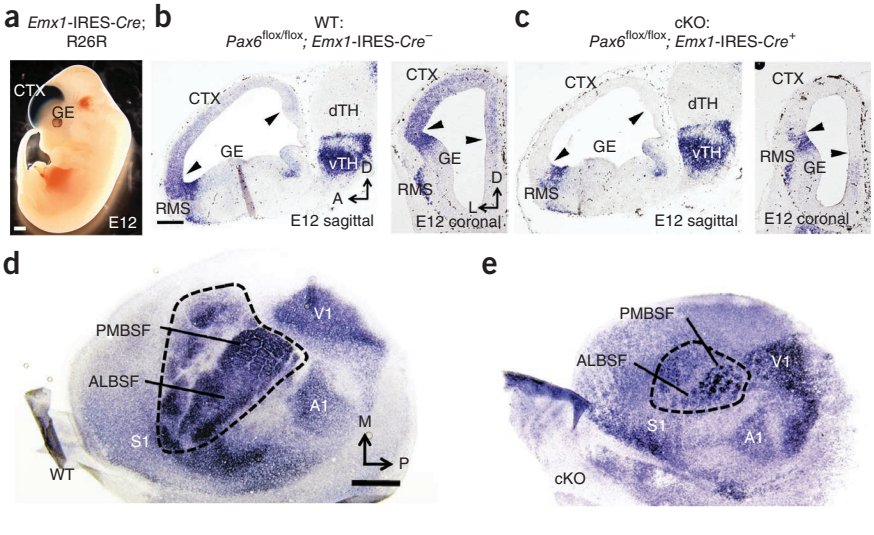

Figure 1 Pax6 specifies S1-area identity in cortical progenitors and determines S1 size. (**a**) Cre-mediated recombination produced by crossing *Emx1*-IRES-*Cre* mice to mice of the R26R reporter line reveals robust β-galactosidase staining that is restricted to the dorsal telencephalon, including the neocortex, at E12. CTX, cortex; GE, ganglionic eminence. (**b**) *In situ* hybridization (ISH) for *Pax6* mRNA in *Pax6*$^{flox/flox}$; *Emx1*-IRES-*Cre*$^{-}$ (wild type (WT)) embryos at E12, revealing graded expression of *Pax6* in cortical progenitors (between arrowheads) and strong expression in the rostral migratory stream (RMS) bordering the ganglionic eminence and in the ventral thalamus (vTH). dTH, dorsal thalamus; A, anterior; D, dorsal; L, lateral. (**c**) In *Pax6*$^{flox/flox}$; *Emx1*-IRES-*Cre*$^{+}$ (cKO) embryos at E12, *Pax6* mRNA is selectively deleted from cortical progenitors (between arrowheads) but remains at normal levels in the RMS and vTH. (**d**,**e**) ISH on tangential sections of flattened cortex at P7 for the sensory area marker *Rorb* showing that deletion of *Pax6* from cortical progenitors specifically using *Emx1*-IRES-*Cre* (cKO) mice results in a reduction of S1 size compared to wild-type mice. Dashed lines outline the S1 border, as identified by *Rorb* staining. M, medial; P, posterior; V1, primary visual area; A1, primary auditory area. Scale bars, 0.5 mm. Bar in **b** applies to **c**; bar in **d** applies to **e**.

but small eye mutants have compromising brain defects and die at birth before the emergence of cortical areas. Therefore, to address whether Pax6 determines S1 size, we crossed mice with floxed alleles of *Pax6* (ref. 25) to mice from an *Emx1*–internal ribosome entry site (IRES)-*Cre* line[26] that generates robust recombination selectively in cortical progenitors (**Fig. 1a**) at embryonic day (E) 10.5 (refs. 26,27) to generate viable *Pax6* conditional knockout (cKO) mice[28] with cortex-specific *Pax6* deletion (**Fig. 1b**,**c**). We performed our primary analyses at postnatal day (P) 7, when area patterning can be defined and the critical period for morphological plasticity in the patterning of the somatotopic body map in S1 is over[11,12,15,23].

We used the S1 marker *Rorb* on tangential sections of flattened cortex at P7 to show that the cortical field with S1 properties was substantially reduced in size in cKO mice compared to wild-type mice (**Fig. 1d**,**e**). We confirmed this assessment using serotonin (5HT) immunostaining, which reveals the somatotopic body map that comprises S1, including the primary body representations of the hindpaw, forepaw, lower jaw, posterior medial barrel subfield (PMBSF) and anterior lateral barrel subfield (ALBSF). The PMBSF and ALBSF, which are the most prominent representations in mouse S1 (**Supplementary Fig. 1**), can be accurately delineated and used to exemplify the effects of Pax6 deletion on S1. Even after correction for

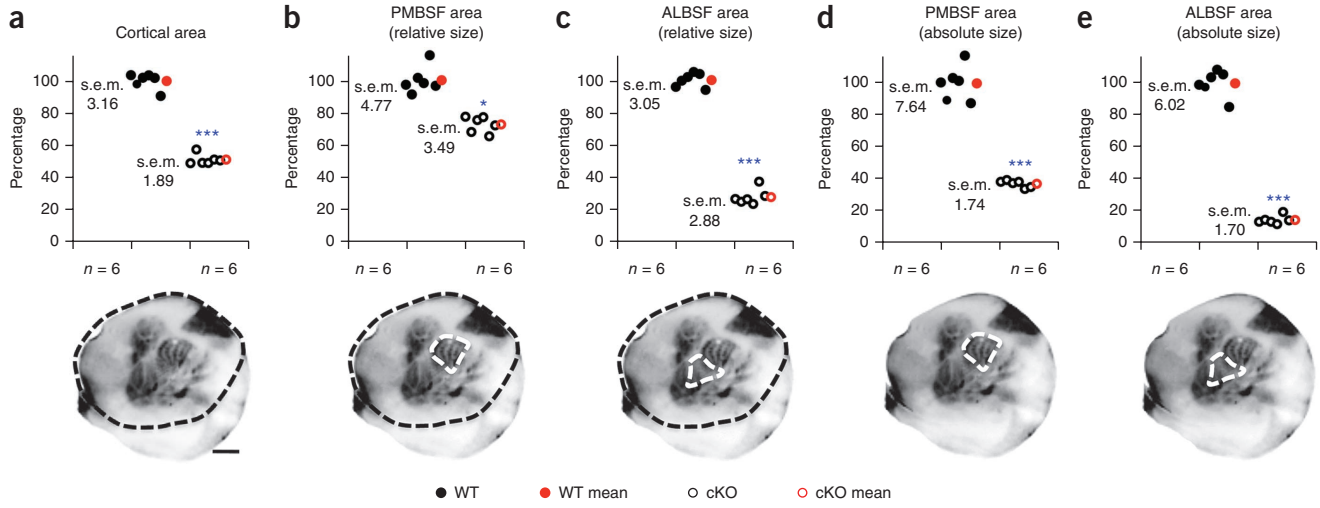

Figure 2 Quantification of the absolute and relative sizes of S1 representations in cKO mice. (**a**–**e**) The neocortical surface area and size of S1 barrel fields quantified at P7 using 5HT staining on tangential sections of flattened cortex. The neocortex of the cKO mice was 51.6% ± 1.89% (mean ± s.e.m.) the size of that of wild-type mice (**a**; $P < 0.0001$, $t = 18.5$, degrees of freedom (df) = 33, $n = 6$). The relative size of the PMBSF of cKO mice was 72.8% ± 3.49% that of wild-type mice (**b**; $P = 0.0015$, $t = 6.3$, df = 5, $n = 6$), and the absolute size of the PMBSF of cKO mice was 37.1% ± 1.74% that of wild-type mice (**d**; $P < 0.0001$, $t = 14.1$, df = 10, $n = 6$). The relative size of the ALBSF of the cKO mice was 27.4% ± 2.88% that of the wild-type mice (**c**; $P < 0.0001$, $t = 38.5$, df = 5, $n = 6$), and the absolute size of the ALBSF of the cKO mice was 14% ± 1.70% that of the wild-type mice (**e**; $P < 0.0001$, $t = 24.1$, df = 10, $n = 6$). $^{*}P < 0.05$; $^{***}P < 0.0001$ (unpaired two-tailed t test). Scale bar, 0.5 mm. Bar in **a** applies to all panels. For relative measurements in **b** and **c**, cortical surface area (black dashed outline) was divided by a given surface area (white dashed outline). For absolute measurements in **d** and **e**, white outlines show the quantified area.

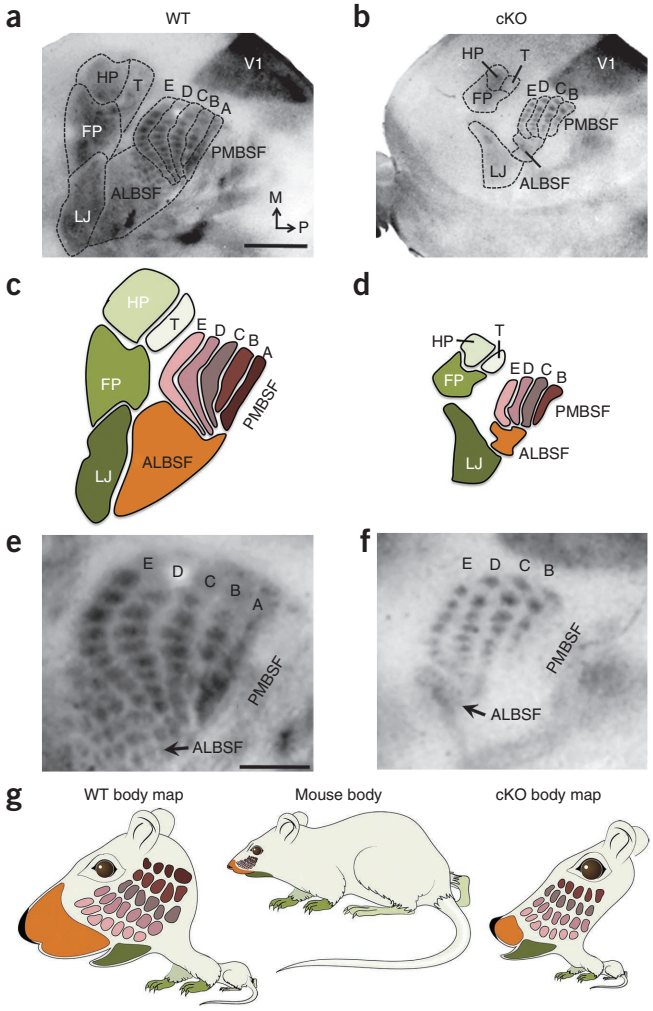

Figure 3 S1 size dictates the resolution and completeness of the body map. (**a**–**d**) 5HT staining of tangential sections of flattened cortex at P7 revealing that all primary components of S1 body map and barrels were miniaturized in cKO mice (**a**,**b**, dashed outlines; **c**,**d**, cartoons). The barrel rows are labeled A–E. HP, hindpaw map; T, map of the trunk and rest of the body; FP, forepaw map; LJ, lower jaw map. (**e**,**f**) Higher magnification of the PMBSF in **a** and **b** (arrows indicate the ALBSF). (**g**) Comparison of the actual mouse body proportions to their representations in the S1 body map illustrating the highly magnified representation of the face, including the small facial whiskers (ALBSF) and the large facial whiskers (PMBSF) on the wild-type body map, compared to the representation of the rest of the body (limbs and trunk). The reduced and incomplete body representations in S1 of cKO mice produce a distorted body map that has abnormal representations of the sensory periphery. Scale bars (**a**,**b**), 0.5 mm; (**e**,**f**), 250 μm.

the reduction in overall cortical size in cKO mice compared to wild-type mice (**Fig. 2a**), both the PMBSF and ALBSF were significantly ($P < 0.001$) reduced in size in cKO mice (**Fig. 2b**,**c**). These findings demonstrate that Pax6 has an important role in specifying S1-area identity in cortical progenitors (**Supplementary Fig. 2**). They also show that *Pax6* cKO mice provide a model to address the effect of reduced S1 size on cortical sensory representations and to determine whether alterations in the cortical body map result in a top-down plasticity in the sensory thalamus and hindbrain.

Reduced S1 contains a miniaturized and incomplete body map

Each of the primary body representations that comprise S1 is substantially reduced in size in cKO mice compared to that in wild-type mice (**Figs. 2** and **3a**–**d**). Quantification showed that the primary representations were reduced in both absolute and relative size but varied substantially in the degree of reduction among the representations. For example, the PMBSF was reduced by 62% in absolute size and 27% in relative size (**Fig. 2b**,**d**), whereas the ALBSF was reduced by 85% in absolute size and 72% in relative size (**Fig. 2c**,**e**). Although the relative measurements demonstrate a role for Pax6 in specifying S1-area identity, the measurements of absolute size are more relevant for the issue of plasticity in sensory circuits and the potential for changes in S1 size and body map to engage a top-down plasticity that may affect VPN and sensory-hindbrain nuclei.

Both the PMBSF and ALBSF are representations of whiskers on the mouse's face and are composed of anatomically discrete, functional units called 'barrels' that are patterned into one-to-one representations that mirror the stereotypic distributions of the facial whiskers[8,15] (**Supplementary Fig. 1**). The PMBSF is the representation of the large facial whiskers (mystacial vibrissae), whereas the ALBSF is the representation of the small facial whiskers on the anterior snout[8]. The PMBSF and ALBSF have the highest magnification factor for any body representation in S1, which is consistent with their behavioral importance to mice and the density of their sensory innervation[6,7,15].

The representation of each body part in S1 was not only substantially reduced in size in cKO mice but also seemed to be incomplete, with the defects in the ALBSF being the most substantial (**Fig. 3a**–**d**). In addition to the near complete loss of the ALBSF, with only 14% ($P < 0.0001$) of this representation persisting in cKO mice, virtually all of the small barrels representing the upper jaw whiskers in the ALBSF of wild-type mice were absent in the ALBSF of cKO mice (**Fig. 3e**,**f**). Significant changes were also evident in the representation of the large facial whiskers in the PMBSF of S1. Consistent with the 62% ($P < 0.0001$) decrease in absolute size of the PMBSF in cKO mice, the individual barrels that comprise it were reduced by 50% (± 4.3% s.e.m., $P < 0.0001$, $t = 17.04$, degrees of freedom = 62, $n = 8$ per genotype) in size on average compared to wild-type mice. In contrast to the five barrel rows in the PMBSF of wild-type mice, we found only four barrel rows in the PMBSF in each of the 28 cKO mice analyzed (**Fig. 3a**–**f**). We identified the missing row to be PMBSF row A by lesioning the C-row whisker follicles on P1 in both wild-type and cKO mice to induce bottom-up plasticity that marked the C row (**Supplementary Fig. 3**). Our findings show that cortex-specific deletion of *Pax6* resulted in an S1 of reduced size, miniaturized representations of body parts in the reduced S1 that varied in degree among the primary presentations and an incomplete representation of the sensory periphery characterized by the reproducible loss of specific parts of the body map (**Fig. 3g**).

The thalamus is repatterned to match S1

The reproducible defects of the body map in S1 of cKO mice provided a model to investigate whether sensory systems have a top-down plasticity that complements the much-studied bottom-up plasticity in a reverse progression[3,4,15,29]. We addressed whether the reduced size of S1 and its incomplete body map in cKO mice were transferred retrogradely through a top-down plasticity from the S1 cortex to the VPN thalamus and perhaps even further down the sensory neuraxis to the trigeminal hindbrain nuclei. To investigate this issue, we analyzed the patterning of VPN thalamus and hindbrain trigeminal nuclei at P7, when cKO mice show an incomplete S1 body map with deletions of specific body representations (**Fig. 3**).

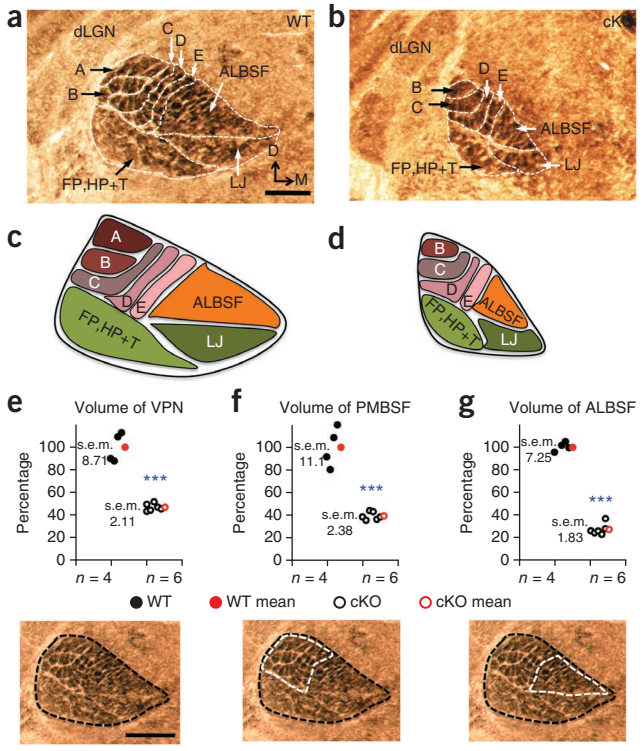

Figure 4 The VPN thalamus was repatterned in cKO mice to match the reduced size and incomplete body map of S1. (**a**,**b**) COX staining on coronal sections at P7 to measure VPN volume and to reveal barreloid patterning. dLGN, dorsal lateral geniculate nucleus; FP,HP+T, barreloids of the paws and the rest of the trunk and body. (**c**,**d**) Schematics of the VPN body maps shown in **a** and **b**. (**e**–**g**) Quantification of the VPN body maps, including VPN volume (**e**; 47.8% ± 2.11% (mean ± s.e.m.) in cKO compared to wild-type mice, $***P < 0.0001$, $t = 9.9$, df = 8, $n = 6$), PMBSF barreloid volume (**f**; 40.08% ± 2.38% in cKO compared to wild-type mice, $***P < 0.0001$, $t = 8.4$, df = 8, $n = 6$) and ALBSF barreloid volume (**g**; 28.62% ± 1.83% in cKO compared to wild-type mice, $***P < 0.0001$, $t = 15.6$, df = 8, $n = 6$). The dashed lines indicate the areas measured, as in **Figure 2**. Scale bars, 250 µm. Bar in **a** applies to **b**; bar in **e** applies to **f**,**g**),

In wild-type mice at P7 (**Fig. 4**), cytochrome oxidase (COX) histochemical staining of coronal sections of the thalamus revealed representations of the forepaws and hindpaws laterally and the lower jaw medially in the ventral VPN and representations of the PMBSF laterally and the ALBSF medially in the dorsal VPN (**Fig. 4a**,**c**). As in the S1 cortex, the PMBSF and the ALBSF were the dominant body representations in the VPN. The PMBSF representation in the VPN was patterned into five rows of discrete 'barreloids' that mirrored the patterning of cortical barrels in the PMBSF of S1 and the large facial whiskers[9] (**Fig. 4a**,**c** and **Supplementary Fig. 1**). In cKO mice at P7, the size of the VPN was reduced to half of that in wild-type mice, paralleling the reduction in S1 size (**Fig. 4e**). COX staining revealed that the somatotopic patterning into the primary representations that was evident in the VPN of wild-type mice was intact in the cKO mice (**Fig. 4a**–**d**), but each representation was markedly reduced in size, which closely approximated their reduction in S1 of cKO mice (compare **Fig. 2d**,**e** to **Fig. 4e**–**g**). For example, the representations of the PMBSF and ALBSF in the VPN were reduced by 60% and 71%, respectively, in the cKO mice at P7, closely paralleling the 62% and 85% reductions, respectively, in the absolute size of these representations in S1. Thus, in cKO mice at P7, the overall size of the VPN and the primary representations in the VPN body map showed significant ($P < 0.0001$) reductions that matched those in their S1 counterparts.

In addition to the substantial reduction in the size of the VPN ALBSF in cKO mice, most of the discrete patterning that was evident in the VPN of wild-type mice was absent in the VPN of cKO mice (**Fig. 4b**,**d**), paralleling the loss of most of the barrels that normally comprise the ALBSF in S1 (**Fig. 3b**,**d**). Similarly to the defects that we identified for the PMBSF in S1 of cKO mice, COX staining of the VPN revealed only four rows of barreloids in cKO mice at P7 (**Fig. 4b**,**d**), with a deletion of row A that corresponded to the absence of row A in the PMBSF of S1 (**Fig. 3e**,**f**). We also used COX staining to investigate whether the defective body maps evident in S1 and VPN of cKO mice were transferred retrogradely to the trigeminal hindbrain nuclei. In contrast to bottom-up plasticity, which induces changes in body maps in a bottom-up progression through the sensory pathway from the hindbrain to the cortex after whisker manipulation[3,4,11,12], both the overall size and completeness of the barrelette representations in the trigeminal sensory hindbrain nuclei were indistinguishable between wild-type and cKO mice (**Fig. 5a**–**d**).

These findings showed that the reduced body map in the S1 cortex of cKO mice at P7 and the selective loss of specific representations were transferred retrogradely to the VPN thalamus, resulting in its repatterning to mirror the aberrant body map in S1. However, this top-down plasticity did not progress further down the sensory neuraxis to the trigeminal hindbrain sensory nuclei, suggesting that the stability of these nuclei and their axonal projections to the VPN had matured beyond the critical period for top-down plasticity or afferent input from the trigeminal ganglia was sufficient to maintain them.

Selective apoptosis repatterns the thalamus

To identify mechanisms responsible for the top-down plasticity in cKO mice that repatterned the VPN to match its size and body map to those of S1, we analyzed the VPN of newborn mice (**Fig. 6**), an age that is early in the development of VPN TCA input to S1 and is during the critical period for bottom-up plasticity[11,12]. Analyses of thalamic architecture using Nissl stain and serotonin immunolabeling showed that the size and appearance of the VPN were similar in

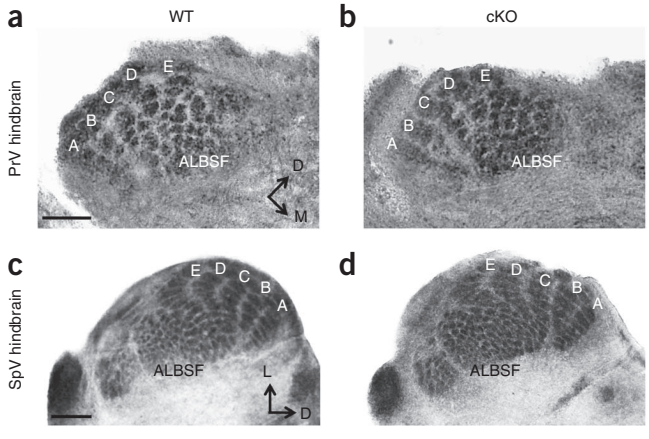

Figure 5 Trigeminal hindbrain nuclei have normal somatotopic patterning in cKO mice. (**a**–**d**) COX staining of coronal sections of the hindbrain through the trigeminal nuclei at P7 revealing indistinguishable barrelette size, number and patterning between WT (**a**,**c**) and cKO (**b**,**d**) mice. PrV, trigeminal principal sensory nucleus; SpV, spinal trigeminal nucleus. Scale bars, 250 µm. Bar in **a** applies to **b**; bar in **c** applies to **d**.

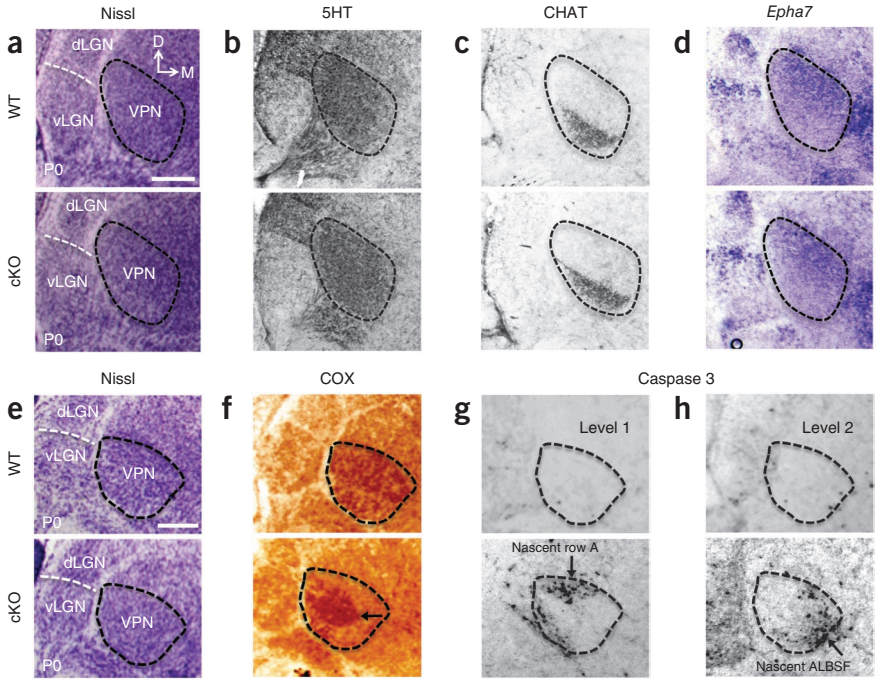

Figure 6 Top-down plasticity repatterns the VPN through exaggerated apoptosis that is selective for VPN neurons representing body parts deleted from S1 in cKO mice. (**a**–**d**) Consecutive coronal sections stained with Nissl (**a**), 5HT (**b**) or choline acetyltransferase antibody (CHAT; **c**) and ISH for *Epha7* (**d**) showing that at P0, before VPN repatterning, cKO mice have similar VPN size and architecture as wild-type mice. vLGN, ventral lateral geniculate nucleus. (**e**–**h**) Consecutive coronal sections stained with Nissl (**e**), histochemically stained for COX (**f**) and stained with antibody to cleaved caspase 3 (**g**,**h**) showing robust COX histochemical staining throughout the VPN and only a few apoptotic neurons positive for cleaved caspase 3 scattered across the VPN. In cKO mice at P0, the VPN resembles that of wild-type mice in size and cell density, as shown with Nissl staining (**e**), but has aberrant COX staining with a robust COX-positive central core (arrow in **f**) surrounded by a COX-negative area that contains dense clusters of caspase 3–positive cells (**g**,**h**) coincident with the representations absent at P7, including row A and most of the ALBSF barreloids (arrows in **g**,**h**). Scale bars (**a**–**h**), 250 μm.

wild-type and cKO mice at P0 (**Fig. 6a**,**b**,**e**). Molecular markers that highlight complementary subdivisions of the VPN, such as choline acetyltransferase, which marks the ventrolateral VPN, and *Epha7*, which marks the dorsomedial VPN, revealed no differences in the molecular patterning of the VPN in wild-type and cKO mice at P0 (**Fig. 6c**,**d**). These findings showed that the initial development of the VPN in cKO mice was similar to that in wild-type mice. Thus, the substantial differences at P7 between the VPN of wild-type and cKO mice were due to a postnatal repatterning of the VPN in cKO mice in response to the reduced size and aberrant body map of S1.

COX staining at P0 revealed the apparent onset of the repatterning of the VPN in cKO mice that was manifested by P7 (**Fig. 4**). COX staining in the VPN is a result of its presence in the mitochondria of VPN neurons and in presynaptic terminals of VPN neurons formed by axons ascending from sensory hindbrain nuclei[15]. In wild-type mice, there was robust COX staining throughout the VPN (**Fig. 6f**). However, in the VPN of cKO mice, robust COX staining was contracted and did not extend throughout the nucleus (**Fig. 6f**). This pattern of COX staining in cKO mice correlated with changes in the body map that became evident at P7: robust COX staining centrally in the VPN was coincident with the nascent representation of the four barreloid rows preserved at P7, whereas low-intensity COX staining at the VPN periphery was coincident with parts of the VPN that contained representations in the VPN body map that were most severely reduced or absent at P7, including the ALBSF and barreloid row A of the PMBSF (compare **Fig. 6f** to the schematics in **Fig. 4c**,**d**). These correlations and the role of COX as an important regulator of oxidative stress[30–32] suggest that COX staining reveals the viability of VPN neurons that represent different body parts and predicts the likelihood of their survival in cKO mice.

These findings indicate that the VPN neurons in cKO mice that would normally form the absent or most severely diminished map representations in S1 were eliminated, resulting in reduced VPN size and repatterning of the VPN body map at P7. To further investigate this issue, we performed immunostaining for cleaved caspase 3, an early apoptotic marker. In wild-type mice at P0, we identified only a few caspase 3–labeled cells scattered over the VPN (**Fig. 6g**,**h**). In contrast, in cKO mice at P0, large numbers of VPN cells were strongly labeled for caspase 3 (**Fig. 6g**,**h**). Rather than being scattered across the VPN, these cells were absent from the domain of robust COX staining in the central VPN and were instead clustered in VPN regions with low-intensity COX staining coincident with the body representations that were the most severely diminished or were absent at P7 in S1 and VPN, including row A of the PMBSF and most of the ALBSF (compare **Fig. 6f**,**h** to **Figs. 3a**–**d** and **4a**–**d**). These findings show that in cKO mice, molecularly normal VPN neurons in regions with abnormally low amounts of COX were eliminated through apoptosis, resulting in a top-down plasticity that reduced and repatterned an initially normally sized and patterned VPN to match the reduced S1 in overall size, resolution and completeness of somatotopic representations in the body map.

TCA competition drives map plasticity

Our findings show that a period of selective and exaggerated apoptosis repatterned the VPN to match the reduced size and incomplete body map of the reduced S1 in cKO mice. We hypothesized that this repatterning process was driven by competitive interactions between TCAs of the VPN neurons in the reduced S1 of cKO mice, with the losers being eliminated. The exaggerated neuronal death in cKO mice was densely concentrated in selective regions of the VPN, leading to the preferential elimination of the body parts they represent (**Supplementary Fig. 2**). Somatotopic patterning and its relationship to specific body parts are assessed and manipulated most readily in the representation of the large facial whiskers in the PMBSF of S1 and VPN[3,4,14,15], leading us to study the PMBSF as a model for mechanisms of top-down plasticity in this sensory system.

Our findings revealed a mechanism acting in the reduced S1 of cKO mice that favored the selective elimination of specific body map components, such as the entire barrel row A in the PMBSF, rather than miniaturizing all map components equally. We hypothesized that this mechanism was based on competitive interactions among VPN TCAs[33], with the competitiveness of TCAs depending on the relative timing of differentiation of their body representations in S1. This competition would be exaggerated in the reduced S1 of cKO

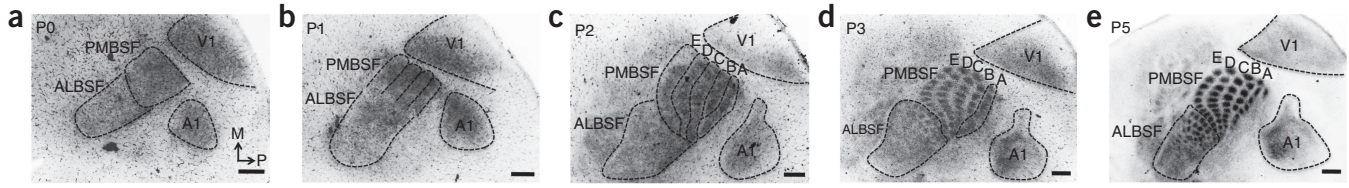

Figure 7 Late differentiation of VPN TCA representations of PMBSF row A and the ALBSF in S1. (**a**–**e**) Spatiotemporal progression of the differentiation of body representations formed by TCAs from the VPN in the cortical plate of S1 analyzed by GFP immunohistochemistry of tangential sections of flattened cortex from *Rora*-IRES-*Cre*; *ROSA26-GAP43-eGFP* mice (**Supplementary Fig. 4**). (**a**) At P0, more GFP-positive TCAs are evident in the nascent PMBSF compared to the future ALBSF, which is still sparsely innervated by GFP-positive TCAs. (**b**) Although not yet segregated by septa, bands of the nascent rostral barrel rows B, C, D and E are evident at P1. (**c**) TCAs forming the immature band for the nascent caudal row A differentiate in the S1 cortical plate later and are first visible at P2. (**d**) By P3, septa between individual barrels of rows B–E and the lateralmost ALBSF barrels are formed and fully differentiated. Conversely, row A still appears as a band. (**e**) Individually separated row-A barrels with differentiated septa are first identifiable at P5. P0, $n = 8$ brains analyzed; P1, $n = 9$; P2, $n = 8$; P3, $n = 8$; P5, $n = 7$. Scale bars (**a**–**e**), 250 µm.

mice, which we predicted would result in the preferential elimination of VPN TCAs that formed later-differentiating representations in S1 followed by the death of their parent VPN neurons and the loss of the same body representations in the VPN. To test this model, we first examined the timing of the ingrowth of VPN TCAs into S1 and the differentiation of their S1 body representations.

For this analysis we used a conditional genetic labeling technique to reproducibly label TCAs projecting from the sensory thalamic nuclei including VPN to cortex, which we visualized using GFP immunostaining by crossing mice from a *Rora*-IRES-*Cre* line[34] to mice from a *ROSA26-GAP43*–enhanced *GFP* (*eGFP*) line carrying a conditionally activated axon reporter[35]. During the first postnatal week, when TCA projections are developing[36,37], mice from the *Rora*-IRES-*Cre* line produced robust recombination throughout the VPN but not in neocortex[34] and therefore GFP immunolabeling in S1 selectively labeled VPN TCAs (**Supplementary Fig. 4**). Using this labeling approach, we found that barrel row A was the last of the five rows in the PMBSF to differentiate (**Fig. 7a**–**e**), which is consistent with previous studies on the developmental differentiation of the PMBSF in rats[38,39] and mice[40]. Similarly, other representations of the body map that were most severely diminished in the cKO mice—for example, the ALBSF—tended to differentiate later (**Fig. 7a**–**e** and refs. 38–40). These findings support our hypothesis that the timing of differentiation of distinct representations in the S1 body map formed by VPN TCAs dictate the competitive balance among them and the selectivity of the representations most severely affected in the cKO body map in S1 and VPN.

Previous studies have shown that competitive interactions between VPN TCAs can be manipulated during a critical period early in the first postnatal week by lesioning whisker follicles on the face, which induces a bottom-up plasticity that ascends the somatosensory pathway to S1 (refs. 3,4,11–13). VPN TCAs representing the lesioned follicles are at a competitive disadvantage, resulting in a reduction in the size of their terminations and corresponding barrels in S1 PMBSF and the possible loss of some VPN neurons representing the lesioned follicles[41]. Therefore, to test whether enhanced competition among VPN TCAs in the reduced S1 of cKO mice resulted in the selective loss of barrel row A, we lesioned the follicles of whisker row C on the faces of wild-type and cKO mice within hours of birth and analyzed the patterning of the S1 PMBSF at P7 using serotonin immunostaining on tangential sections of flattened cortices. These early lesions done at P0 induced a stronger bottom-up plasticity than lesions done at P1 to identify rows in the S1 PMBSF (**Supplementary Fig. 3**).

In unlesioned cKO mice at P7, four distinct rows of barrels (B–D) were evident, and although the barrels were smaller than those in the S1 PMBSF of wild-type mice at P7, they were clear and present in normal numbers (compare **Fig. 8a** to **Fig. 3b**,**d**,**f**). In contrast, in cKO mice at P7 that had the C row of whisker follicles lesioned early on P0, the C row in the S1 PMBSF was virtually absent and had few barrels evident (**Fig. 8b**). Coincident with this strong bottom-up plasticity, the lesion done at P0 also resulted in a clear, albeit partial, rescue of row A in the PMBSF of S1 that was evident in cKO mice at P7 (**Fig. 8b**). We conclude that this deprivation of C-row input to S1 altered the competitive balance among VPN TCAs and placed those representing row C at a competitive disadvantage, leading to their virtual elimination from S1 of cKO mice and allowing TCAs representing the A row to compete more effectively for space in the reduced S1, which permitted a partial rescue of the A row representation.

Increasing S1 size rescues the body map

Our findings suggest that the incomplete body map in the reduced S1 of cKO mice was due to an exaggerated competition among VPN TCAs for limited cortical space that was inadequate to accommodate

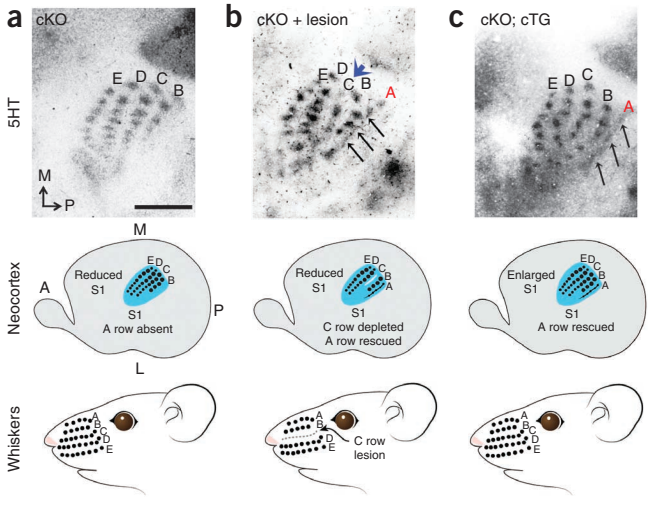

Figure 8 Altering the competitive balance among VPN TCAs rescues representations deleted from S1 body map in cKO mice. (**a**) 5HT staining of tangential sections of flattened cortex at P7 showing that only four barrel rows are evident in the PMBSF in S1 in cKO mice, with row A absent. (**b**) Lesioning the C row of large facial whisker follicles in cKO mice within a few hours of birth diminishes the C barrel row in S1 (blue arrowhead) and partially rescues VPN TCA input to row A in the S1 PMBSF (black arrows), resulting in five rows in the PMBSF, as in wild-type mice, compared to four PMBSF rows in unlesioned cKO mice. (**c**) Increasing the size of S1 in *Pax6* cKO mice by cortex-specific expression of a *Pax6* transgene (cKO; cTG mice) also partially rescues the A row in the PMBSF of S1. Scale bar (**a**–**c**), 250 µm.

the complete body representation. To further test this notion, we complemented the follicle-lesion experiment with a cortex-specific genetic approach designed to increase the size of the reduced S1 in cKO mice, and we predicted that this would rescue the missing body representations. For this approach, we created a new conditional *Pax6* transgenic line (*nestin-Pax6cTG*), and by crossing mice from this new line to mice from the *Emx1*-IRES-*Cre line*[26], we were able to selectively activate ectopic *Pax6* in the same cortical progenitors in which endogenous *Pax6* was conditionally deleted in the cKO mice (**Supplementary Fig. 5**). We focused our analyses on the PMBSF of S1 in cKO mice and in cKO mice crossed to *nestin-Pax6cTG* mice (cKO; cTG mice).

Activation of the *Pax6* transgene in cKO; cTG mice resulted in a significant ($P = 0.0004$) ~20% increase in PMBSF size in S1 compared to cKO mice (**Supplementary Fig. 6**). At P7, the cKO; cTG mice showed a partial, but clear, rescue of row A in the PMBSF (**Fig. 8c**). In contrast to what we found in the follicle-lesion experiment (**Fig. 8b**), the other four PMBSF rows were unaffected and had the same appearance as those in S1 of cKO mice (**Fig. 8b,c**). These findings support our conclusion that S1 size has a substantial influence on competitive interactions among VPN TCAs in S1 and their ability to survive; therefore, S1 size is a crucial parameter in determining the completeness of the cortical body map.

DISCUSSION

We exploited features of the mouse somatosensory system that led to its prominence as a model for sensory map development and bottom-up plasticity and used this system to show the consequences of reduced cortical area size on the representation of the sensory periphery and reveal a top-down plasticity that is driven by competition-mediated axon elimination and neuronal apoptosis. We found that cortex-specific deletion of *Pax6* resulted in an S1 with a substantially reduced size, showing that Pax6 is required in specifying S1-area identity in cortical progenitors. The reduction in S1 size resulted in a miniaturized body map in the reduced S1 and a reproducible loss of specific representations of the sensory periphery from the S1 body map. Thus, genetic mechanisms intrinsic to the cortex place strict limitations on the physical dimensions of the cortical field that TCAs from the VPN thalamus are able to innervate, thereby determining the overall size, resolution and completeness of the S1 body map. This intrinsic limitation resulted in a defective S1 body map and engaged a top-down plasticity that repatterned the VPN thalamus retrogradely to match the reduced size of S1 and its aberrant body map. Before its repatterning, the VPN thalamus had a normal size and normal molecular differentiation, but its repatterning in cKO mice was predicted by differential amounts of COX activity, which correlate with the metabolic health and viability of neurons[30–32], and molecularly normal VPN neurons with abnormally low amounts of COX were selectively eliminated through apoptotic cell death. A potentially diminished number of layer six corticothalamic axons[36,37] may have also contributed to the reduction in VPN size in cKO mice.

Our findings in cKO mice reveal a mechanism that favors the reproducible elimination of selective parts of the body map rather than miniaturizing all map components equally. This mechanism is initiated by the preferential elimination of VPN TCAs that represent specific body parts from the reduced S1 and was manifested by an exaggerated apoptosis of VPN neurons that were densely concentrated in selective regions of the VPN rather than being more uniformly distributed across the nucleus. This mechanism seemed to be based on a competitive balance among VPN TCAs that was determined by the relative timing of differentiation of the body representations that they formed in S1, with TCAs that form later-differentiating representations being preferentially excluded from S1 and their parent neurons being deleted from the VPN. This competitive model for top-down plasticity and its selectivity was further supported by two sets of experiments in cKO mice that showed that altering the competitive imbalance among VPN TCAs rescues representations in the S1 body map that are otherwise selectively eliminated, either by inducing classic bottom-up plasticity through peripheral sensory deprivation or by a transgenic approach intrinsic to the cortex that partially restores the size of the genetically reduced S1.

We conclude that S1 size modulates competitive interactions among VPN TCAs, influencing the organization, resolution and completeness of the S1 body map that they form, which in turn initiates a top-down plasticity that drives the repatterning of the VPN thalamus through axon elimination and cell death to match the reduced size of S1 and its aberrant body map. It is probable that the reduced size of S1 diminished not only the space available for the termination of VPN TCAs but also the trophic support for them and their parent neurons. We propose that during normal development, these mechanisms tune sensory maps in the cortex and thalamus and account for the precise matching in thalamocortical and corticothalamic circuits that is required for the proper function of sensory systems. The mechanisms demonstrated here can produce relatively minor adjustments in sensory maps, as well as the more substantial adjustments that are required by the prominent disparity in the sizes of primary sensory areas that is present even among the normal population[16–18] but that is exaggerated in individuals with certain neurogenetic disorders[20,42].

Potential roles for top-down plasticity complement those proposed for bottom-up plasticity in tuning sensory components in the brain, with the sensory periphery accounting for normal and abnormal variations in their size and organization. Our findings lead us to speculate that size differences in sensory areas in humans above a critical threshold may have pathological consequences. For example, in autism spectrum disorder (ASD), large-scale changes in the cortical gene expression profile that controls area patterning[43] coincide with massive expansion of the frontal cortex[42,44], but the overall cortical surface area shows little change in these individuals, implying that the more posteriorly positioned sensory cortical areas, including S1, are reduced in size, which may lead to defects in their sensory maps that resemble those in the reduced S1 of cKO mice. In addition, these changes in the sensory cortex would probably engage top-down plasticity and lead to similar defects in the sensory thalamus, which is consistent with a reduction in thalamic volume in individuals with ASD[45,46]. Neurodevelopmental mechanisms, including intrinsic neocortical area patterning and top-down plasticity and their consequences, may contribute to the complex pathologies of ASD and other sensory processing disorders.

METHODS

Methods and any associated references are available in the online version of the paper.

Note: Supplementary information is available in the online version of the paper.

ACKNOWLEDGMENTS

We thank B. Higgins and H. Gutierrez for technical assistance, J. Simon (Salk Institute MultiMedia Resources) for help making Adobe Illustrator schematics, Y. Dayn (Salk Institute Transgenic Core) for help producing the *nestin-Pax6TG* conditional transgenic mice, K. Jones (University of Colorado) for the *Emx1*-IRES-*cre* mice, M. Goulding (Salk Institute) for the *ROSA26-GAP43-eGFP* mice and members of the O'Leary lab for discussion. This work was supported by US National Institutes of Health grants R01 NS31558 and R01 MH086147 and the Vincent J. Coates Chair of Molecular Neurobiology (D.D.M.O.).

AUTHOR CONTRIBUTIONS

A.Z. and D.D.M.O. designed the study, analyzed findings, prepared figures and wrote the paper. A.Z. performed the primary experiments. S.-J.C. and D.D.M.O. designed and generated the *nestin-Pax6TG* conditional transgenic mice. R.A.-P. and A.S. designed and generated the *Pax6* cKO mice. All authors read and approved the final manuscript.

COMPETING FINANCIAL INTERESTS

The authors declare no competing financial interests.

1. Kaas, J.H. The evolution of complex sensory systems in mammals. *J. Exp. Biol.* **146**, 165–176 (1989).
2. Krubitzer, L. & Kahn, D.M. Nature versus nurture revisited: an old idea with a new twist. *Prog. Neurobiol.* **70**, 33–52 (2003).
3. Erzurumlu, R.S., Murakami, Y. & Rijli, F.M. Mapping the face in the somatosensory brainstem. *Nat. Rev. Neurosci.* **11**, 252–263 (2010).
4. Erzurumlu, R.S. & Gaspar, P. Development and critical period plasticity of the barrel cortex. *Eur. J. Neurosci.* **35**, 1540–1553 (2012).
5. Krubitzer, L.A. & Seelke, A.M. Cortical evolution in mammals: the bane and beauty of phenotypic variability. *Proc. Natl. Acad. Sci. USA* **109** (suppl. 1): 10647–10654 (2012).
6. Krubitzer, L. & Kaas, J. The evolution of the neocortex in mammals: how is phenotypic diversity generated? *Curr. Opin. Neurobiol.* **15**, 444–453 (2005).
7. Krubitzer, L. In search of a unifying theory of complex brain evolution. *Ann. NY Acad. Sci.* **1156**, 44–67 (2009).
8. Woolsey, T.A. & Van der Loos, H. The structural organization of layer IV in the somatosensory region (SI) of mouse cerebral cortex. The description of a cortical field composed of discrete cytoarchitectonic units. *Brain Res.* **17**, 205–242 (1970).
9. Van Der Loos, H. Barreloids in mouse somatosensory thalamus. *Neurosci. Lett.* **2**, 1–6 (1976).
10. Ma, P.M. & Woolsey, T.A. Cytoarchitectonic correlates of the vibrissae in the medullary trigeminal complex of the mouse. *Brain Res.* **306**, 374–379 (1984).
11. Belford, G.R. & Killackey, H.P. The sensitive period in the development of the trigeminal system of the neonatal rat. *J. Comp. Neurol.* **193**, 335–350 (1980).
12. Durham, D. & Woolsey, T.A. Effects of neonatal whisker lesions on mouse central trigeminal pathways. *J. Comp. Neurol.* **223**, 424–447 (1984).
13. Feldman, D.E., Nicoll, R.A. & Malenka, R.C. Synaptic plasticity at thalamocortical synapses in developing rat somatosensory cortex: LTP, LTD, and silent synapses. *J. Neurobiol.* **41**, 92–101 (1999).
14. Fox, K. & Wong, R.O. A comparison of experience-dependent plasticity in the visual and somatosensory systems. *Neuron* **48**, 465–477 (2005).
15. Fox, K. *Barrel Cortex* (Cambridge University Press, 2008).
16. Andrews, T.J., Halpern, S.D. & Purves, D. Correlated size variations in human visual cortex, lateral geniculate nucleus, and optic tract. *J. Neurosci.* **17**, 2859–2868 (1997).
17. White, L.E. *et al.* Structure of the human sensorimotor system. II: lateral symmetry. *Cereb. Cortex* **7**, 31–47 (1997).
18. Dougherty, R.F. *et al.* Visual field representations and locations of visual areas V1/2/3 in human visual cortex. *J. Vis.* **3**, 586–598 (2003).
19. Higginbotham, H., Yokota, Y. & Anton, E.S. Strategies for analyzing neuronal progenitor development and neuronal migration in the developing cerebral cortex. *Cereb. Cortex* **21**, 1465–1474 (2011).
20. Rubenstein, J.L. Annual research review: development of the cerebral cortex: implications for neurodevelopmental disorders. *J. Child Psychol. Psychiatry* **52**, 339–355 (2011).
21. Leingärtner, A. *et al.* Cortical area size dictates performance at modality-specific behaviors. *Proc. Natl. Acad. Sci. USA* **104**, 4153–4158 (2007).
22. Zhou, L. *et al.* Maturation of "neocortex isole" *in vivo* in mice. *J. Neurosci.* **30**, 7928–7939 (2010).
23. O'Leary, D.D., Chou, S.J. & Sahara, S. Area patterning of the mammalian cortex. *Neuron* **56**, 252–269 (2007).
24. Bishop, K.M., Goudreau, G. & O'Leary, D.D. Regulation of area identity in the mammalian neocortex by Emx2 and Pax6. *Science* **288**, 344–349 (2000).
25. Ashery-Padan, R., Marquardt, T., Zhou, X. & Gruss, P. Pax6 activity in the lens primordium is required for lens formation and for correct placement of a single retina in the eye. *Genes Dev.* **14**, 2701–2711 (2000).
26. Gorski, J.A. *et al.* Cortical excitatory neurons and glia, but not GABAergic neurons, are produced in the Emx1-expressing lineage. *J. Neurosci.* **22**, 6309–6314 (2002).
27. Chou, S.J., Perez-Garcia, C.G., Kroll, T.T. & O'Leary, D.D. Lhx2 specifies regional fate in Emx1 lineage of telencephalic progenitors generating cerebral cortex. *Nat. Neurosci.* **12**, 1381–1389 (2009).
28. Piñon, M.C., Tuoc, T.C., Ashery-Padan, R., Molnar, Z. & Stoykova, A. Altered molecular regionalization and normal thalamocortical connections in cortex-specific Pax6 knock-out mice. *J. Neurosci.* **28**, 8724–8734 (2008).
29. Petersen, C.C. The functional organization of the barrel cortex. *Neuron* **56**, 339–355 (2007).
30. Diaz, F. Cytochrome c oxidase deficiency: patients and animal models. *Biochim. Biophys. Acta* **1802**, 100–110 (2010).
31. Diaz, F., Garcia, S., Padgett, K.R. & Moraes, C.T. A defect in the mitochondrial complex III, but not complex IV, triggers early ROS-dependent damage in defined brain regions. *Hum. Mol. Genet.* **21**, 5066–5077 (2012).
32. Hüttemann, M. *et al.* Regulation of mitochondrial respiration and apoptosis through cell signaling: cytochrome c oxidase and cytochrome c in ischemia/reperfusion injury and inflammation. *Biochim. Biophys. Acta* **1817**, 598–609 (2012).
33. Wallace, H. & Fox, K. Local cortical interactions determine the form of cortical plasticity. *J. Neurobiol.* **41**, 58–63 (1999).
34. Chou, S. *et al.* Geniculocortical input drives genetic distinctions between primary and higher-order visual areas. *Science* **340**, 1239–1242 (2013).
35. Sapir, T. *et al.* Pax6 and engrailed 1 regulate two distinct aspects of renshaw cell development. *J. Neurosci.* **24**, 1255–1264 (2004).
36. Grant, E., Hoerder-Suabedissen, A. & Molnar, Z. Development of the corticothalamic projections. *Front. Neurosci.* **6**, 53 (2012).
37. Molnár, Z., Garel, S., Lopez-Bendito, G., Maness, P. & Price, D.J. Mechanisms controlling the guidance of thalamocortical axons through the embryonic forebrain. *Eur. J. Neurosci.* **35**, 1573–1585 (2012).
38. Rhoades, R.W. *et al.* Development and lesion induced reorganization of the cortical representation of the rat's body surface as revealed by immunocytochemistry for serotonin. *J. Comp. Neurol.* **293**, 190–207 (1990).
39. Schlaggar, B.L. & O'Leary, D.D. Early development of the somatotopic map and barrel patterning in rat somatosensory cortex. *J. Comp. Neurol.* **346**, 80–96 (1994).
40. Vitalis, T. *et al.* Effects of monoamine oxidase A inhibition on barrel formation in the mouse somatosensory cortex: determination of a sensitive developmental period. *J. Comp. Neurol.* **393**, 169–184 (1998).
41. Waite, P.M., Li, L. & Ashwell, K.W. Developmental and lesion induced cell death in the rat ventrobasal complex. *Neuroreport* **3**, 485–488 (1992).
42. Courchesne, E. *et al.* Mapping early brain development in autism. *Neuron* **56**, 399–413 (2007).
43. Voineagu, I. *et al.* Transcriptomic analysis of autistic brain reveals convergent molecular pathology. *Nature* **474**, 380–384 (2011).
44. Courchesne, E. *et al.* Neuron number and size in prefrontal cortex of children with autism. *J. Am. Med. Assoc.* **306**, 2001–2010 (2011).
45. Tamura, R., Kitamura, H., Endo, T., Hasegawa, N. & Someya, T. Reduced thalamic volume observed across different subgroups of autism spectrum disorders. *Psychiatry Res.* **184**, 186–188 (2010).
46. Cheon, K.A. *et al.* Involvement of the anterior thalamic radiation in boys with high functioning autism spectrum disorders: a diffusion tensor imaging study. *Brain Res.* **1417**, 77–86 (2011).

ONLINE METHODS

Mouse lines. All experiments were approved and conducted following the guidelines of the Institutional Animal Care and Use Committee at the Salk Institute and were in full compliance with the guidelines of the US National Institutes of Health for the care and use of laboratory animals. Analyses were done independent of sex and included both male and female mice according to Mendelian ratios. The background strain was C57BL/6. Cortex-specific *Pax6* knockout mice (called here cKO mice) were generated by crossing *Pax6*-floxed ($Pax6^{flox/flox}$) mice[25] with *Emx1*-IRES-*Cre*–expressing mice[26] as described[28]. *Pax6* transgenic mice (called here cTG mice) were generated by pronuclear injection into fertilized oocytes. To limit activation to neuronal progenitors, the *Pax6* transgene included a CNS-specific enhancer from the second intron of the *nestin* gene[47] that was subcloned upstream of the *Hsp68* promoter driving a stop cassette (comprised of an *eGFP* reporter, a stop codon and three tandem poly(A) sequences) that was flanked by *loxP* sites, followed by *Pax6* cDNA (**Supplementary Fig. 5**). Transgenic founders were backcrossed on the C57BL/6 background and screened for germline transmission. To generate dorsal thalamus–specific reporter mice and label TCAs, *Rora*-IRES-*Cre* transgenic mice[34] were crossed to *GAP43-eGFP* reporter mice[35], termed *Rora-Cre-GAP43-eGFP* mice. Mice lacking endogenous Pax6 in cortical progenitors but expressing ectopic Pax6 from the conditional transgene (called here cKO; cTG mice) were generated by crossing cKO mice to cTG mice. To assess the specificity of *Cre* recombination in mouse embryos, *lacZ* reporter mice expressing *lacZ* under the *ROSA26* (R26R) promoter[48] were crossed to mice expressing *Emx1*-IRES-*Cre*[26]. Genotyping was done by PCR using primers for *Pax6*-floxed alleles (FLP6/83: GCG-GTT-GAG-TAG-CTC-AAT-TCT-A, FLP6/84: AGT GGC-TTG-GAC-TCC-TCA-AGA, FLP6/del: CGT-GTG-CCC-CAG-CTT-CCG-GT), *Cre* (*cre* forward: ATG-CTT-CTG-TCC-GTT-TGC-CG, *cre* reverse: CCT-GTT-TTG-CAC-GTT-CAC-CG), *GFP* (*GFP* forward: GAC-GTA-AAC-GGC-CAC-AAG-TT, *GFP* reverse: GAA-CTC-CAG-CAG-GAC-CAT-GT), *nestin-Pax6TG* (*Hsp* forward: TTC-AGA-ACT-GTG-GGA-GTT-GG, *Pax6* reverse: TAG-CCA-GGT-TGC-GAA-GAA-CTC-TGT) and *lacZ* (β-galactosidase) (*lacZ* forward: TTG-GCG-TAA-GTG-AAG-CGA-C, *lacZ* reverse: AGC-GGC-TGA-TGT-TGA-ACT-G).

ISH, immunostaining, LacZ staining, tangential sections and COX histochemistry. Mice were perfused with 4% phosphate-buffered paraformaldehyde (PFA), washed in PBS and cryoprotected in 30% sucrose in PBS. Brains were embedded in Tissue-Tek Optimal Cutting Temperature (OCT) compound (Sakura Finetek) and sectioned on a Cryostat (Leica). Antisense RNA probes for *Rorb*, *Pax6* and *Epha7* were labeled using a digoxigenin RNA labeling kit (Roche). ISH and immunostaining on 18-µm cryostat sections were carried out as previously described[49]. For tangential sections, cortical hemispheres were dissected, flattened and post-fixed between slide glasses and then cryoprotected. Tangential sections were cut at 40 µm from flattened cortical hemispheres and stained for *Rorb* or serotonin. For Nissl staining, sections were stained with 0.5% cresyl violet and then dehydrated with graded alcohols. Immunohistochemistry was performed on 18-µm coronal or sagittal or 40-µm tangential cryosections. Antigens were unmasked by boiling in citrate buffer (Vector). The primary antibodies used were to serotonin (1:20,000, Immunostar, 20080, http://www.immunostar.com/antibody/5-ht-serotonin-rabbit-antibody/), ChAT (1:1,000, Chemicon, AB144P, http://www.millipore.com/catalogue/item/ab144p), cleaved caspase 3 (1:400, Cell Signaling, 9661, http://www.cellsignal.com/products/9661.html) and GFP (1:1,000, Molecular Probes, A11122, http://products.invitrogen.com/ivgn/product/A11122/. Primary antibodies were incubated overnight at 4 °C in blocking solution containing 3% bovine serum albumin (Fisher Scientific) and 0.1% Tween-20 (Sigma) in PBS. Biotinylated secondary antibodies (goat anti-rabbit, 1:500, Jackson ImmunoResearch, 111-065-144; horse anti-goat, 1:500, Vector, BA-9500) were incubated for 45 min at room temperature. For immunostaining, sections were developed following the Vectastain standard diaminobenzidine (DAB) colorimetric reaction kit (Vector). LacZ staining was performed on E12 whole-mount embryos. β-galactosidase activity was developed in staining solution (PBS, 1 mg ml^{-1} X-gal, 2 mM $MgCl_2$, 0.01% SDS, 0.02% NP-40, 5 mM $K_3Fe(CN)_6$ and 5 mM $K_4Fe(CN)_6$) for 2–6 h at 30 °C. Specimens were then washed in PBS and post-fixed in PFA. COX histochemistry was performed on fixed, 18-µm cryosections as described previously[21]. Sections were incubated overnight at 37 °C in 0.1 M phosphate buffer containing 5% sucrose, 0.03% cytochrome *c*, 0.02% catalase and 0.05% DAB.

Whisker lesion. Mice, within hours of birth or at P1, were anesthetized by cooling. The central C whisker row was identified under a surgical microscope, and whiskers including the follicles were plucked using scalpels and tweezers. Mice were revived on a 37 °C heating pad and returned to their home cages. At P7, the mouse brains were dissected and processed for serotonin staining on tangential sections.

Measurements and statistical analyses. Data collection and analyses were performed blind to genotype and the conditions of the experiments, data were collected and processed randomly, and no data points were excluded. No statistical methods were used to predetermine sample sizes, but our sample sizes were similar to those reported in previous publications (for example, refs. 38,40). Data met the assumptions of the statistical tests used, and the data distribution was assumed to be normal but was not formally tested. Statistics were calculated with Microsoft Excel. Quantifications show individual data points and the mean values of the tested groups and are displayed as a percentage of the wild-type group. Analyzed numbers of brains (*n*) for each set of experiments are indicated in the corresponding figures and figure legends or main text sections. The examples shown in each figure are representative and were reproducible for each set of experiments. Individual experiments were successfully repeated at least five times using different litters. Statistical significance was determined using unpaired two-tailed *t* test, $P < 0.05$ (*) was considered statistically significant, $P < 0.001$ was considered highly statistically significant (**) and $P < 0.0001$ was considered extremely statistically significant (***). Variance is indicated in the figure graphs and figure legends and was calculated using the s.e.m. Absolute and relative neocortical surface areas and the size of cortical barrel fields stained with serotonin or *Rorb* was measured using ImageJ[50], as shown in the schematic drawings in **Figures 2** and **4** and **Supplementary Figure 6**. The volume of the VPN and barreloid subfields was measured on series of consecutive 18-µm COX-stained coronal sections using ImageJ[50].

47. Yaworsky, P.J. & Kappen, C. Heterogeneity of neural progenitor cells revealed by enhancers in the nestin gene. *Dev. Biol.* **205**, 309–321 (1999).
48. Soriano, P. Generalized lacZ expression with the ROSA26 Cre reporter strain. *Nat. Genet.* **21**, 70–71 (1999).
49. Zembrzycki, A., Griesel, G., Stoykova, A. & Mansouri, A. Genetic interplay between the transcription factors Sp8 and Emx2 in the patterning of the forebrain. *Neural Dev.* **2**, 8 (2007).
50. Rasband, W.S. ImageJ. US National Institutes of Health, Bethesda, Maryland, USA ⟨http://imagej.nih.gov/ij/⟩ (1997–2013).

doi:10.1038/nn.3454